NASA Technical Memorandum 79323

(NASA-TM-79323) LASER ANEMCMETER MEASUREMENTS IN A TRANSONIC AXIAL FLOW COMPRESSOR ROTOR (NASA) 17 p HC A02/MF A01 CSCL 01A

N80-14050

Unclas

G3/02 46440

LASER ANEMOMETER MEASUREMENTS IN A TRANSONIC AXIAL FLOW COMPRESSOR ROTOR

Anthony J. Strazisar and
J. Anthony Powell
Lewis Research Center
Cleveland, Ohio

Prepared for the
Twenty-fifth Annual International Gas Turbine Conference and
the Twenty-second Annual Fluids Engineering Conference
sponsored by the American Society of Mechanical Engineers
New Orleans, Louisiana, March 9-13, 1980

E-279

LASER ANEMOMETER MEASUREMENTS IN A TRANSONIC AXIAL FLOW COMPRESSOR ROTOR

Anthony J. Strazisar and J. Anthony Powell
National Aeronautics and Space Administration
Lewis Research Center
Cleveland, Ohio

ABSTRACT

A laser anomometer system employing an efficient data acquisition technique has been used to make measurements upstream, within, and downstream of the compressor rotor. A fluorescent dye technique allowed measurements within endwall boundary layers. Adjustable laser beam orientation minimized shadowed regions and enabled radial velocity measurements outside of the blade row. The flow phenomena investigated include flow variations from passage to passage, the rotor shock system, three-dimensional flows in the blade wake, and the development of the outer endwall boundary layer. Laser anemometer measurements are compared to a numerical solution of the streamfunction equations and to measurements made with conventional instrumentation.

INTRODUCTION

Advances in the aerodynamic technology of turbomachinery are dependent on obtaining a comprehensive understanding of the complex physical phenomena which occur within the blade passages. Progress is being attained through improvements in both analytic and experimental techniques. With the increased availability of large scale computers significant advances in computational methods for compressor design and analysis are being made. As advances in numerical methods continue, there is an increasing need to make detailed flow measurements inside blade rows. Such measurements will determine flow phenomena such as the distribution of turning and losses which are required inputs for some numerical methods. They will also generate data for use in verifying numerical solutions.

Cascade tests and the use of rotating instrumentation in low-speed machines are two experimental approaches to the measurement of intra-blade flowfields. However, these approaches cannot provide data on the combined effects of high Mach number and high rotational speeds. High-response pressure measurements and non-intrusive optical measurement techniques such as laser anemometry and holographic interferometry are extending flow measurement capabilities in the high-speed testing regime beyond those available with conventional low-response instrumentation. Applications of laser anemometer (LA) systems to axial-flow turbomachinery employing fringe-type anemometers have been reported in [1-3]. Applications involving time-of-flight anemometers have been reported in [4].

This paper describes the application of a LA system to a transonic axial-flow compressor rotor. The results of several types of measurements which demonstrate the system's capability of measuring velocity and flow angle in a rotating blade row are discussed. However a comprehensive evaluation of the flow in this transonic compressor is beyond the scope of the present paper. A detailed description of this LA system is contained in [5]. Since transonic compressor testing requires a significant expenditure of both manpower and energy, a rapid data acquisition technique has been developed in order to minimize running time. The incorporation of four degrees of freedom in the laser beam orientation enables measurement of the radial component of velocity in some cases and the minimization of regions blocked from optical access by the complex blade geometry.

TEST COMPRESSOR AND INSTRUMENTATION

The test rotor of the present study was designed as an inlet rotor for a core compressor. The rotor design pressure ratio and mass flow are 1.67 and 215 kg/m^2/s, respectively, at a tip speed of 426 m/s. The tip relative Mach number is 1.4 at design speed. The rotor has 52 blades, a tip chord length of 44.6 mm, and a tip solidity of 1.48. The inlet tip diameter is 508 mm and the hub-tip radius ratio is 0.7. For the LA application reported herein, the rotor was tested without inlet guide vanes and without a stator blade row. This configuration eliminates the circumferential variation in the flowfield induced by the stationary blade rows and thereby simplifies data acquisition and analysis.

Optical access is provided by a glass window which is 102 mm long in the axial direction and 51 mm wide (11 degrees arc) in the circumferential direction. The window material is 3 mm thick commercial window glass formed to the outer endwall contour. Static blade tip clearance was set at 1 mm under the window. Window washing is performed about once an hour during compressor operation by injecting automative window washing fluid into the endwall boundary layer through a row of 0.5 mm holes located 230 mm upstream of the window.

Laser anemometer measurements were made along the design streamsurfaces shown in Fig. 1. Measurements are distributed at axial locations between $z = -25.4$ mm and $z = 50.8$ mm as shown along streamsurface 2. Conventional probe survey measurements were made at stations 1 and 2 using a 6.4 mm diameter combination probe. The probe used contains a thermocouple, total pressure tube, and null balancing static pressure holes for measurement of total temperature, total pressure, and flow angle. Details of the conventional survey data acquisition and reduction system are given in [6]. The operating points at which LA surveys were performed are shown in the performance map for the rotor as measured using the conventional instrumentation (Fig. 2).

LASER ANEMOMETER SYSTEM

The laser anemometer is a single-channel, dual-beam system with on-axis backscatter light collection. The LA system optical layout is shown in Fig. 3. The laser light source is a 1.6 W argon-ion laser operating at 514.5 nm. The beam crossing angle is 2.825 degrees and the fringe spacing is 10.4 μm. The probe volume diameter based on the $1/e^2$ intensity points is 125 μm. The length of common intersection of the crossing beams is about 4 mm. The effective length of the probe volume is reduced to about 2 mm by placing a mask on the central portion of the focusing lens located in front of the photomultiplier tube. Backscatter light is collected through an 11 degree cone angle.

The entire optical system is mounted on an x-y traversing table which is used to set the probe volume axial and radial position. A rotatable beam splitter is used to rotate the plane of the laser beams for measurement of velocity components at various angles from the axial direction. The beams nominally enter the compressor rotor in the radial direction. A beam director mirror is used to direct the beam away from the radial direction by ±10 degrees to minimize shadowed regions caused by blade twist as shown in Fig. 4. Without variable beam direction, 20% to 30% of the blade-to-blade passage at the hub would be blocked due to blade twist at sections AA and BB. Another advantage offered by the variable beam direction is that it gives some capability of measuring radial velocity components.

Measurements to within 1 mm of the endwalls are made possible by using a fluorescent dye seed material and an optical filter. Without the fluorescent seed, reflected light from the endwall surfaces prevents measurements at radial positions less than 10 mm from either endwall. Seed particles are generated by spray-atomization and are injected into the inlet through a 6.4 mm diameter tube located 460 mm upstream of the rotor face. The seed material consists of rhodamine 6G dye dissolved in a benzyl alcohol, ethylene glycol solution [7]. When a seed particle containing this dye crosses the LA fringe system the particle absorbs the green incident light and fluoresces orange. An orange-pass filter placed in front of the photomultiplier tube optically filters out green light reflected from blade and endwall surfaces and passes orange light scattered from the seed particles.

DATA ACQUISITION

The data acquisition technique is efficient in that it allows free-running of the LA system. Unlike several other LA systems used in turbomachinery research [1,3,4], the optical system is not gated by a once-per-rev or once-per-blade signal, but is free to make velocity measurements whenever a seed particle crosses the probe volume. The technique is implemented by using a dedicated minicomputer to control data acquisition. The seed particle fringe crossing frequency (which is proportional to the particle velocity) is measured by a commercial counter-type processor. The rotor shaft position is generated by an electronic shaft angle encoder which provides a continuous measure of the rotor shaft position relative to a once-per-rev signal obtained from the rotor disk. When a velocity measurement occurs the minicomputer records the frequency and shaft position as a data pair. At each axial and radial position surveyed, data are recorded at 1000 different shaft positions. These positions are typically distributed as 50 positions per blade passage across 20 consecutive blade passages.

It is significant that the velocity measurements do not really occur at a discrete shaft position, but rather are made anywhere within an interval between adjacent rotor shaft positions marked by the shaft angle encoder. With 50 intervals per blade passage, the interval length varies between 0.43 mm at the hub and 0.61 mm at the tip of the blade. In this paper the term 'shaft position' is used with the understanding that measurements attributed to a shaft position actually occur in an interval about that position.

A typical run consists of collecting 30,000 measurements yielding an average of 30 measurements at each shaft position. Run times typically vary between 15 and 45 seconds. During data acquisition a graphics terminal is used to generate a graphic display which is typically updated every 15 seconds based on the data accumulated to that point in the run. The display consists of a histogram of the number of measurements at each shaft position and a blade-to-blade velocity distribution averaged across the 20 measured blade passages along the circumferential measurement path. This real-time display adds to the efficiency of the system since it enables the operator to monitor the data acquisiton process and terminate a run if necessary. At the conclusion of each run, a data table of N_j, $\sum_{i=1}^{N_j} f_i$, $\sum_{i=1}^{N_j} f_i^2$ is stored on disk. Subscript j is the shaft position number which runs from 1 to 1000, N is the total number of measurements at position j, and f_i is the LA signal frequency of the i^{th} measurement at position j. Further details of the data acquisition system can be found in reference [5].

DATA REDUCTION

The measured particle fringe crossing frequency is converted to velocity by multiplying by the fringe spacing. The velocity is corrected to standard day conditions using the relation

$$V_c = V\sqrt{T_s/T_p},$$

where V_c is the corrected velocity, T_p is the temperature measured in a plenum chamber upstream of the compressor inlet, and T_s is the standard-day temperature. For each measured component of velocity the mean and standard deviation at each shaft position are then calculated from

$$\bar{V} = \sum_{i=1}^{N} V_i/N$$

$$V' = \left[\left(\sum_{i=1}^{N}\left(V_i - \bar{V}\right)^2\right)\Big/(N-1)\right]^{1/2}$$

$$= \left[\left(\sum_{i=1}^{N} V_i^2 - N\bar{V}^2\right)\Big/(N-1)\right]^{1/2}$$

The velocity magnitude and flow angle are calculated at each position using data from runs made at different beam orientations. The geometry of the beam orientation is shown in Fig. 5. The measured velocity component V_m lies along line AA which is in the plane of the beams and perpendicular to the bisector of the crossing beams. The beam bisector can be deflected in an off-radial direction by the beam director mirror. The beam bisector is restricted to the (R,θ) plane and the deflection angle is denoted by ϕ_r. The rotatable beam splitter is used to rotate the direction of the fringe normals about the R'-axis (which is alined with the beam bisector). The angle between the fringe normals and the Z-axis is denoted by ϕ_z and is measured in the (Z,θ') plane. The mean and standard deviation of the z,θ,r velocity components are calculated from the three equations

$$V_z \cos \alpha_i + V_\theta \cos \beta_i + V_r \cos \gamma_i = V_{m_i} \qquad i = 1,2,3$$

where subscript i denotes each different beam orientation and

$$\cos \alpha = \cos \phi_z$$

$$\cos \beta = \cos \phi_r \sin \phi_z$$

$$\cos \gamma = \sin \phi_r \sin \phi_z$$

The two equations

$$V_z \cos \alpha_i + V_\theta \cos \beta_i = V_{m_i} \qquad i = 1,2$$

can be used to calculate V_z and V_θ using data obtained during two runs made at different ϕ_z angles with $\phi_r = 0$. In practice the ϕ_r angles for the two runs are equal but are set to some non-zero value in the range ±4 degrees to minimize the blade shadow regions. Thus the calculated V_θ component of velocity actually lies along the θ' direction. However, the difference between the calculated velocity in the θ' direction and the velocity in the θ direction is small compared to the measurement error since the cosine of four degrees is 0.9976.

The velocity distribution across the 20 measured blade passages is considered to be 20 separate observations of the flow in an average blade passage. Velocities at corresponding points relative to the blade in each individual blade passage are averaged together to yield a spatially-ensemble averaged blade-to-blade velocity distribution. The averaged velocity distribution may be compared to the velocity distribution in individual blade passages to assess passage-to-passage flow variations.

MEASUREMENT ERRORS

The error in axial and radial probe volume positioning is ±0.05 mm. The errors in setting the beam splitter and beam director angles are ±0.03 degree and ±0.01 degree, respectively. The error in a single LA measurement is a function of flow turbulence intensity and random noise in the photomultiplier tube signal. It is difficult to make an error estimate for an individual measurement since this noise is generated by background radiation which varies with each measurement. However, the statistical confidence in N individual measurements made at a given shaft position is

$$k = cV' \Big/ \left(\bar{V}\sqrt{N}\right),$$

where k is the length of the confidence interval and c is the confidence level. N is approximately 30 for each point in the velocity distribution across an individual blade passage. N is approximately 600 for each point in the ensemble-averaged velocity distribution, since the averaged distribution is calculated from the 20 individual blade-to-blade velocity distributions. All error bars which appear in this paper are for a 95% confidence level ($c = 2$). It should be noted that V' results from the sum of the flow fluctuation effects such as those caused by turbulence, velocity variations due to rotor speed drift, and velocity gradients in the tangential direction across the measurement shaft position interval. plus the previously mentioned random noise in the photomultiplier tube signal. The maximum velocity gradient in the tangential direction occurs across the passage shock during transonic operating conditions and is on the order of 1% per shaft position interval. Observations indicate that the rotor speed drift during a run is on the order of 0.3%.

Least squares polynomial curves are fit to the data prior to comparing velocity distributions. One advantage to this approach is that the fitted curve contains information from all 1500 measurements made in a blade passage (30 measurements at each of 50 points), while the data at a single shaft position are based on only about 30 measurements. Typically the difference between the data and the fitted curve is 1% to 2%.

Two additional sources of measurement error are statistical and angle biasing. Statistical biasing arises because of the following. First, the velocity magnitude varies with time. Second, for a uniformly seeded flow more particles cross the probe volume per unit time when the velocity is higher than the mean than when the velocity is lower than the mean. An arithmetic average of measurements made over a given period of time therefore yields a calculated mean velocity which is higher than the true mean. Statistical bias can be removed using the relation [8]

$$\bar{V} = \bar{V}_b \Big/ \left[1 + \left(V'/\bar{V}\right)_b^2\right]$$

where subscript b denotes biased measurements. Typical values for $(V'/\bar{V})_b$ outside of blade wake and shock regions are 3% to 6%, which result in a 0.4% correction. Because this correction is small, the data have not been corrected for statistical bias.

Angle biasing [9] occurs because the flow direction fluctuates with time. More measurements per unit occur when the flow direction is parallel to the fringe normal direction than when the flow direction fluctuates away from the fringe normal direction. The error in an arithmetic average of the velocity measurements made over a given time period is proportional to the angle between the fringe normals and the mean flow direction. This error is 1% or less when the angle between the fringe normals and the mean flow direction is less than 20 degrees. In the present work the ϕ_z fringe orientation angle is set at ±15 degrees from the average flow angle to minimize angle biasing error. However, the flow angle changes by 30 degrees across wakes and passage shocks. Therefore there are regions in which the angle between the fringe normals and the velocity vector is on the order of 45 degrees which could result in a 4% error in the measured velocity.

SEED PARTICLE DYNAMICS

The rotor passage shock can be used to determine particle lag and seed particle size using the method described in [3]. A Stokes drag model is used to predict the velocity response downstream of the shock for a particle of diameter D_p. The resulting equation is

$$18\, \nu_g x_n / D_p (\rho_p/\rho_g) = (C_1 - C_2) - C_2 \ln\left[(V_n - C_2)\big/(C_1 - C_2)\right] - (V_n - C_2)$$

where

C_1 = pre-shock gas velocity normal to the shock in the (Z,θ) plane

C_2 = post-shock gas velocity normal to the shock in the (Z,θ) plane

V_n = particle velocity component normal to the shock in the (Z,θ) plane

$= V_{REL} \sin(\beta_{REL} + \alpha)$

x_n = particle distance normal to the shock

$= s \cos \alpha$

The relative flow angle β_{REL} and the shock inclination angle α are defined in Fig. 6. The measured velocity component V_n as a function of x_n is determined from the ensemble-averaged blade-to-blade distribution of relative velocity V_{REL} using the geometry shown in Fig. 6, where s is the distance downstream of the shock along the circumferential measurement path. This procedure assumes that the distribution of V_n is uniform along the face of the shock over the distance $s \cdot \sin \alpha$. Typical values of s and α used in the above calculations are 14 mm and 10 degrees, respectively, which yield $s \cdot \sin \alpha = 2.4$ mm.

The particle diameter D_p is determined in the following manner: For various values of D_p, V_n is calculated at given values of x_n using the known values of ρ_p, ρ_g, ν_g, C_1, and C_2. The particle diameter is then taken as the value of D_p which yields the best agreement between the calculated and measured distribution of V_n as a function of x_n. The results of two particle size determinations are shown in Fig. 7. Each data point in the figure is based on approximately 600 measurements. The data were obtained under identical flow and signal processor conditions at two different axial stations. The only change made in the LA system between the two runs was the removal of the orange filter used in the fluorescent dye technique. The agreement between the data obtained at axial stations $z = 10.2$ mm and $z = 12.7$ mm indicates that V_n is uniform along the face of the shock over distances of 2 to 3 mm. With the orange filter in place, the minimum diameter of the particles detected by the optics is about 1.4 µm, while the diameter of particles detected without the filter in place is 1.2 µm. This difference in diameter reflects the loss in signal strength in passing through the orange filter. With the LA counter-processor threshold level held constant, a larger particle diameter is necessary to trigger the counter circuitry when the filter is in place.

The results shown in Fig. 7 indicate that the distance required for the particle velocity to decay to within 5% of the post-shock gas velocity is about 12 mm normal to the shock. This is about 13 mm or 13% of the blade chord in the relative flow direction. Note that the flow angle as well as the velocity magnitude is in error in the lag region. Additional particle size determinations performed with the orange filter in place yield particle sizes ranging from 1.2 to 1.5 µm. Although the minimum particle size detected by the optics increases with the orange filter in place, comparisons of blade-to-blade velocity distributions measured under identical flow conditions with and without the filter in place indicate no differences greater than the experimental error in the velocity distribution results due to the use of the filter.

The passage shock is not the only region in the blade passage where particle tracking may be a problem. Maxwell [10] analyzed seed particle flow in an axial-flow compressor rotor similar to the test rotor used in the present study. He obtained a numerical solution for the gas flowfield and then integrated the particle equation of motion to determine the particle path and velocity. The results indicate that for 1.5 µm diameter particles the particle-to-gas velocity ratios are $0.90 < V_p/V_g < 0.96$ in the leading edge region and $0.98 < V_p/V_g < 1.02$ through the remainder of the blade passage. Particle angular deviation was found to be a maximum of 6 degrees along the suction surface and across the blade passage at the trailing edge.

RESULTS AND DISCUSSION

Flow phenomena studied during the initial application of the LA system include variations in flow from passage-to-passage, shock surface location, velocity changes across shock waves, three-dimensional flows in the blade wake, and the development of the endwall boundary layer. In addition, LA measurements were compared to numerical results within the blade row and to conventional probe measurements at stations outside of the blade row. The results obtained will be briefly discussed.

Passage-to-Passage Flow Variations

One advantage of the current data acquisition scheme is the ability to record velocity measurements across consecutive individual blade passages. Passage-to-passage variations in flow conditions can be observed and analyzed by using data from the individual blade passages. As an example, the distribution of absolute velocity across five consecutive blade passages is shown in Fig. 8 at four axial stations (given in percent axial chord) along streamsurface 1 (near the tip). The operating point is near stall at 75% of design speed. At -25% and 2% chord the flow in passage 9 is clearly different from that in passages 8 and 10. The variation in flow between passages at 2% chord may be caused by small variations in leading edge geometry and axial location. Least squares curve fits of the velocity distribution in passages 8 and 9 are compared to curve fits of the averaged velocity distribution in Fig. 9 where the blade locations are denoted by the cross-hatched areas. The error bars in Fig. 9 represent twice the standard deviation between the fitted curve and the data and therefore encompass 95% of the data points. Using the averaged curve fit as a reference, we see that the flow variation between passages 8 and 9 is a maximum of 20% near the leading edge. The data shown here represent the greatest passage-to-passage velocity variation observed in the present work. At operating points near maximum efficiency the incidence angles are small and there is less turning around the blade leading edge relative to that for the near stall case. Passage-to-passage flow variations at these operating points are on the order of 5% or less.

Blade-to-Blade Velocity Distributions

It is generally desirable to use the ensemble-averaged velocity distributions when performing data analyses because the ensemble-averaged data set, which contains 50 points in the averaged velocity distribution, is much smaller than the unaveraged data set which contains 1000 points in the velocity distributions across 20 blade passages. A possible source of error in using the averaged data is the tendency to smear out details of the velocity distribution by averaging across the 20 blade passages. However, comparison of the averaged and unaveraged distributions in Fig. 9, a worst-case example, indicates that velocity distribution details are not significantly modified by averaging.

Ensemble-averaged blade-to-blade distributions of velocity and flow angle measured on streamsurface 1 (near the tip) at 23% chord under transonic operating conditions are shown in Fig. 10. The operating point is at design speed near stall mass flow. The passage shock location is indicated gy the rapid change in velocity and flow angle at mid-passage. Note that the absolute flow remains axial until it encounters the shock even though the measurement station is located well behind the leading edge. The shock turns the absolute flow by more than 30 degrees which represents 75% of the turning measured at the blade trailing edge.

Rotor Shock Surface Mapping

The three-dimensionality of the rotor shock system is shown graphically in Fig. 11 where the shock location on streamsurfaces 1,2,3 (near-tip, mid-span, and near-hub, respectively) is plotted for the maximum mass flow condition at 100% design speed. The inlet relative Mach number varies from 1.16 on the near-hub streamsurface to 1.39 on the near-tip streamsurface. The blade sections and shocks are radially projected to eliminate the spanwise variation of blade spacing. The shock location is determined from velocity distributions of the type shown in Fig. 10. The flow behind the passage shock is supersonic on all three streamsurfaces. At mid-span and near the hub (streamsurfaces 2 and 3, respectively) the flow then diffuses to subsonic velocities within the blade passage without passing through another shock. However on streamsurface 1 (near the tip) the flow passes through a normal shock near the blade trailing edge.

The swept back blade leading edge creates a shock surface which leans back in the flow direction from hub to tip. Flow turning across the inclined shock in the meridional plane generates an increase in the radial velocity component toward the tip downstream of the shock. As noted in [2,4], the values of relative velocity and flow angle measured across the shock do not satisfy the isentropic normal shock relations even after correction for particle lag effects. It is found that an outward radial velocity component upstream of the shock must be assumed in order to satisfy the shock relations. The corresponding calculated streamline slope just upstream of the shock in the meridional plane is on the order of 40 degrees. The calculations are sensitive to velocity magnitude and flow angle and to shock inclination angle in the meridional plane. A 2% to 3% deviation in velocity results in a 15% deviation in the calculated streamline slope. Although attempts to measure the radial velocity component near the passage shock were not successful, a strong deposition of seed particles was observed on the window in the outer casing around the passage shock region. This may indicate that a radial outward flow is present in the vicinity of the shock.

Rotor Wake Measurements

Averaged velocity distributions measured downstream of the rotor at 70% design speed and at both maximum efficiency and near-stall conditions are shown in Fig. 12. The measurements were made on streamsurface 1 (near the tip), at station 2. The averaged velocity distribution is repeated so that the wake appears in the center of each plot. The radial velocity V_r and streamline slope in the meridional plane α_s are defined as positive outward toward the tip. The streamline slope outside of the wake agrees with the design streamline slope of -12 degrees. Outward radial velocities in the blade wake are to be expected due to the radial pressure imbalance on the wake fluid. The radial outward flow, relative velocity defect, and wake width are all larger at the near-stall point than at the maximum efficiency operating point.

Endwall Boundary Layer Development

The development of the outer endwall boundary layer at design speed and maximum mass flow is shown in Fig. 13. The effective probe volume length of 2 mm is indicated in the figure. The velocity at each data point is obtained by arithmetically averaging all 30,000 measurements obtained along the circumferential measurement path. The spanwise location of each point is the location of the probe volume center. Averaging across the finite probe volume length results in measured velocities which are higher than the true velocity, particularly near the wall. The boundary layer downstream of the blade is thinner than that upstream of the blade. This thinning of the boundary layer reflects the energy addition which occurs in passing through the rotor.

Comparison of LA Measurements and Numerical Results

The results of a finite difference solution [11] of the streamfunction equation on streamsurface 2 are compared to LA measurements in Fig. 14. The measurements were performed at 70% design speed near the maximum efficiency operating point. The cross-hatched areas near the blade surface denote regions in which no measurements were obtained. The numerical and experimental results display reasonable agreement in the expansion region around the blade leading edge, but the LA measurements indicate less diffusion than predicted by the numerical solution near the pressure side of the blade passage in the rear portion of the passage. This behavior may be due to the fact that the numerical model is inviscid and therefore cannot account for the displacement thickness effect of the blade wakes.

Comparison of LA and Conventional Probe Measurements

LA measurements are compared to conventional pressure survey measurements at stations 1 and 2 (see Fig. 1). The conventional instrumentation measures velocity and flow angle averaged along the entire circumference at a given axial and radial positon. All 30,000 LA measurements obtained along a circumferential measurement path are therefore arithmetically averaged for comparison with the conventional survey measurements. The LA and conventional measurements are not made simultaneously since different compressor casings are used for the LA and survey runs, and measurement repeatability is therefore a factor to be considered in comparing results. The measurement repeatability of each instrumentation system when the compressor rig conditions are not changed is 1%. The repeatability in resetting the compressor rig conditions is 2%. Two additional factors which affect the comparison of results are the presence of a seed injection probe wake during LA measurements and probe blockage effects during pressure survey measurements. Although the seed injection probe is located 72 probe diameters upstream of station 1, a limited number of LA surveys made at station 1 in the θ-direction indicate that a 2% to 4% velocity defect from the seed injection probe is present at station 1. During pressure survey measurements there are four probes each at stations 1 and 2 and eight additional probes downstream of station 2. When the probes are fully extended for measurements near the hub, the total frontal area for the four probes at each station is 2% of the annulus area at the rotor face. An observed decrease in wall static pressures during probe injection indicates that throughflow velocity variations due to probe injection do exist.

The LA measurements of absolute velocity and flow angle at station 1 agree with the pressure survey measurements to within 4%. This is considered reasonable in view of the factors discussed above. The absolute velocities measured at station 2 by the LA and survey probe agree within 7%, but the flow angles measured by the two systems disagree by as much as 14%. The disagreement between the measured flow angles is due to differences in the measured V_θ velocity component. Agreement between the V_z velocity component measured by the LA and the survey probe is comparable to the agreement at station 1, but the V_θ component measured by the LA is 10% to 15% lower than that measured by the survey probe. The reasons for this difference require further study.

SUMMARY AND CONCLUDING REMARKS

The application of a laser anemometer system to the measurement of flow in a transonic axial flow compressor rotor is described. Use of a dedicated minicomputer to control data acquisition allows rapid accumulation of data with high spatial resolution in the blade-to-blade direction and the recording of data across 20 individual blade passages. A fluorescent dye technique reduces problems due to incident light reflection from metal blade passage surfaces and allows measurements to be made in the endwall boundary layers. The ability to direct the input laser beams away from the radial direction allows minimization of blade blockage effects and enables the measurement of radial velocity components.

Future research plans include holographic interferometric studies of the rotor shock system. Shock patterns measured by the holographic technique will be compared to those measured by the LA. Future LA research will involve measurements in compressor stages with stator blades present so that both rotor and stator flowfields and the extent of the circumferential variations in the rotor flowfield induced by the stator may be investigated. Survey probe and LA measurements will be made simultaneously to further investigate differences between the velocities measured by the two systems and to investigate the significance of survey probe blockage effects.

ACKNOWLEDGEMENTS

The authors wish to acknowledge the contributions of Genevieve Esgar for running the numerical streamfunction solutions used in comparison with the LA data and of Mark Laessig for assisting in data reduction and analysis.

NOMENCLATURE

c	confidence interval
C_1	pre-shock gas velocity normal to the passage shock in the (Z,θ) plane
C_2	post-shock gas velocity normal to the passage shock in the (Z,θ) plane
D_p	seed particle diameter
f	seed particle fringe crossing frequency
k	confidence interval length
N	number of measurements
PR	total pressure ratio across the rotor
PS	blade pressure surface
r	radial distance
s	distance along circumferential measurement path
SS	blade suction surface
T_p	plenum temperature
T_s	standard day temperature, 518.7 degrees Rankine
U	wheel speed
V	velocity
V_{ABS}	absolute flow velocity
V_n	particle velocity component normal to the passage shock in the (Z,θ) plane
V_{REL}	relative flow velocity
W	compressor mass flow
x	particle distance normal to the passage shock
z	axial distance
α,β,γ	laser beam orientation angles measured from the z,θ,r axes
α_s	streamline slope in the meridional plane
β_{ABS}	absolute flow angle
β_{REL}	relative flow angle
θ	circumferential distance
ν	kinematic viscosity
ρ	density
ϕ_r	angle between the beam bisector and the radial direction
ϕ_z	angle between the fringe normals and the axial direction

Subscripts:

b	biased
c	corrected to standard day conditions
g	gas
i	denotes i^{th} measurement at a given shaft position
j	shaft position number
m	measured
p	particle
r	radial direction
z	axial direction
θ	tangential direction

Superscripts:

—	denotes mean quantity
′	denotes fluctuating quantities

REFERENCES

1. Wisler, D.C. and Mossey, P.W., "Gas Velocity Measurements Within a Compressor Rotor Passage Using the Laser Doppler Velocimeter," Journal of Engineering for Power, Vol. 95, No. 2, Apr. 1973, pp. 91-96.
2. Wisler, D.C., "Shock Wave and Flow Velocity Measurements in a High Speed Fan Rotor Using the Laser Velocimeter," ASME Paper No. 76-GT-49, Mar. 1976.
3. Walker, D.A., Williams, M.C., and House, R.D., "Interblade Velocity Measurements in a Transonic Fan Utilizing a Laser Doppler Velocimeter," Minnesota Symposium on Laser Anemometry, E.R.G. Eckert, ed., University of Minnesota, Minneapolis, Minn., 1976, pp. 124-145.
4. Dunker, R.J., Strinning, P.E., and Weyer, H.B., "Experimental Study of the Flow Field Within a Transonic Axial Compressor Rotor by Laser Velocimetry and Comparison with Through-Flow Calculations," Journal of Engineering for Power, Vol. 100, No. 2, Apr. 1978, pp. 279-286.

5. Powell, J.A., Strazisar, A.J., and Seasholtz, R.G., "Efficient Laser Anemometer for Intra-Rotor Flow Mapping in Turbomachinery." To be Presented at the Symposium on Measurement Methods in Rotating Components of Turbomachinery; Gas Turbine Conference and Products Show, American Society of Mechanical Engineers, New Orleans, La., March 9-13, 1980.

6. Moore, R.D., Lewis, G.W., Jr., and Osborn, W.M., "Performance of a Transonic Fan Stage Designed for a Low Meridional Velocity Ratio," NASA TP-1298, 1978.

7. Stevenson, W.H., dos Santos, R., and Mettler, S.C., "Fringe Mode Fluoresence Velocimetry," Applications of Non-Instrusive Instrumentation in Fluid Flow Research, AGARD-CP-193, 1976, pp. 20-1-20-9.

8. Barnett, D.O. and Bentley, H.T., "Statistical Bias of Individual Realization Laser Velocimeters," Second International Workshop on Laser Velocimetry, Vol. 1, H.D. Thompson and W.H. Stevenson, eds., Purdue University, 1974, pp. 428-444.

9. Seasholtz, R.G., "Laser Doppler Velocimeter System for Turbine Stator Cascade Studies and Analysis of Statistical Biasing Errors," NASA TN D-8297, 1977.

10. Maxwell, B.R., "Tracer Particle Flow in a Compressor Rotor Passage with Application to LDV," American Institute of Aeronautics and Astronautics Journal, Vol. 13, No. 9, Sept. 1975, pp. 1141-1142.

11. Katsanis, T., "FORTRAN Program for Calculating Transonic Velocities on a Blade-to-Blade Stream Surface of a Turbomachiner," NASA TN D-5427, 1969.

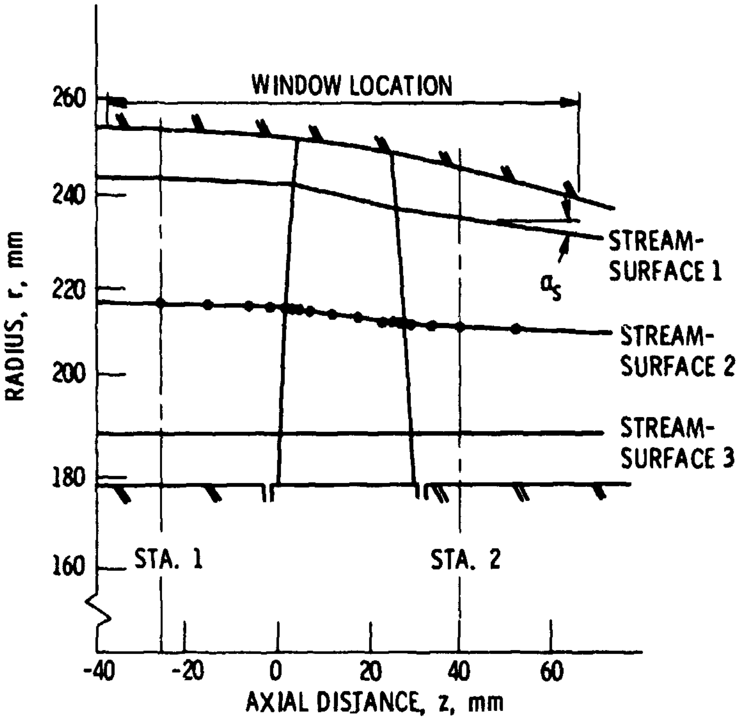

Figure 1. - Test compressor flowpath and streamsurface locations.

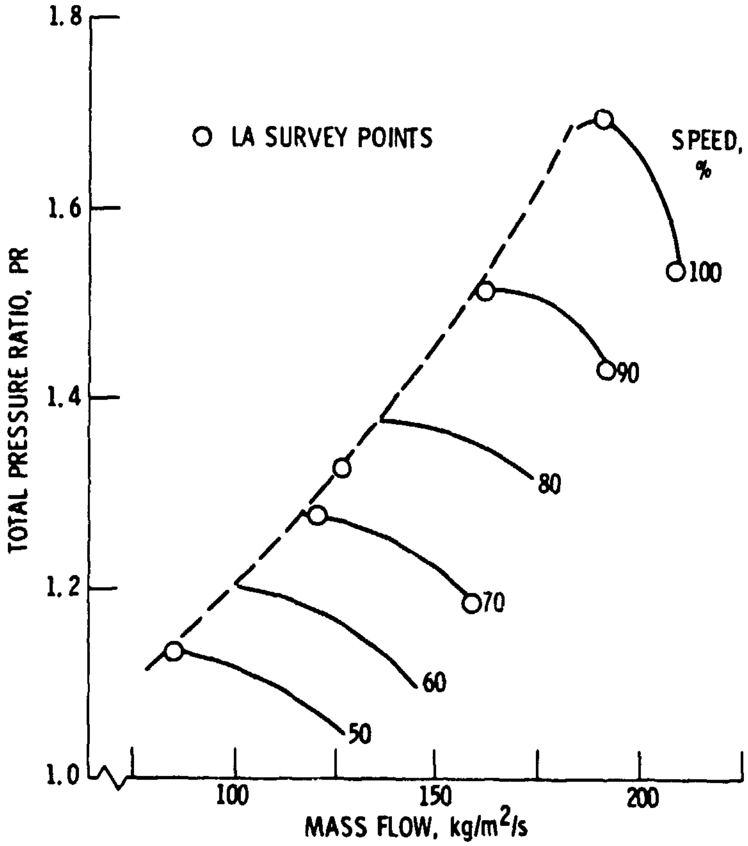

Figure 2. - Test compressor performance map.

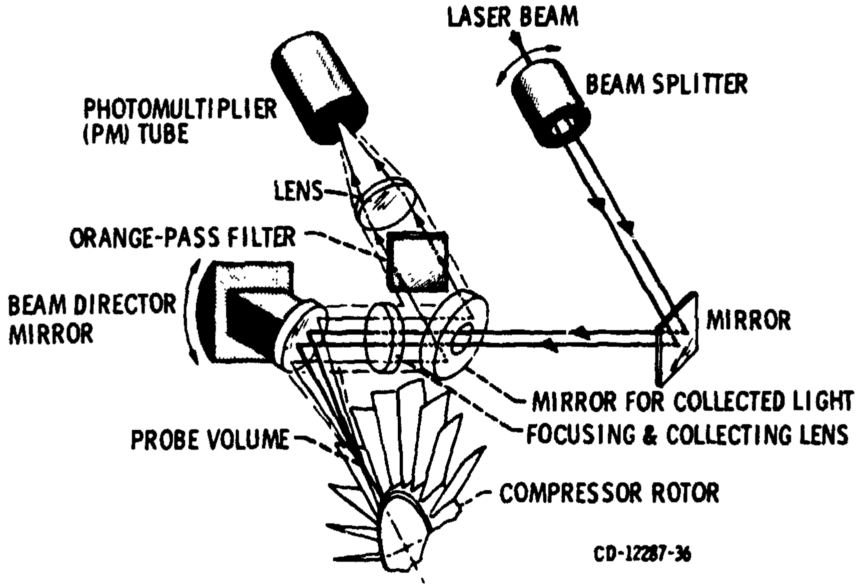

Figure 3. - Laser anemometer system optical layout.

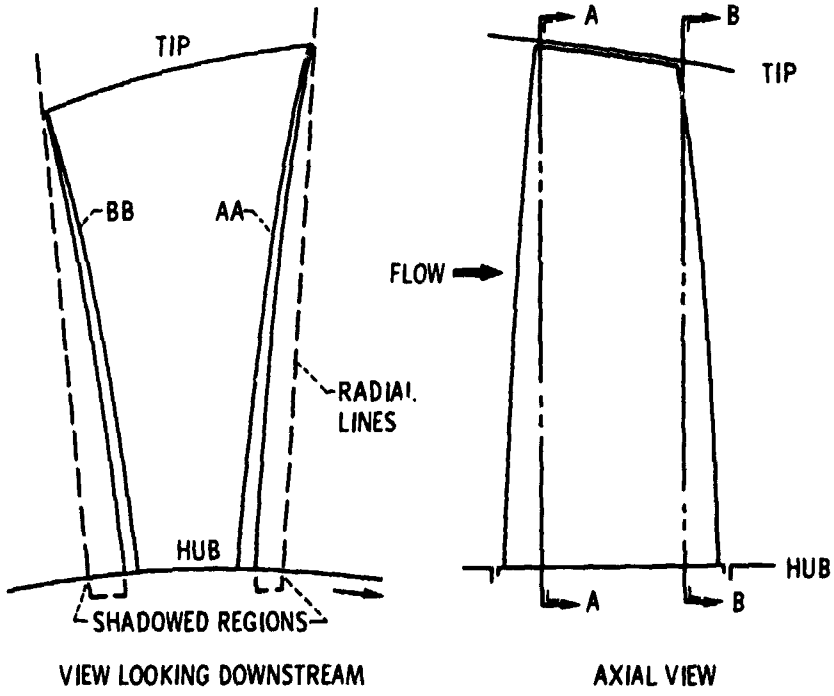

Figure 4. - Blade geometry showing shadowed regions due to blade twist.

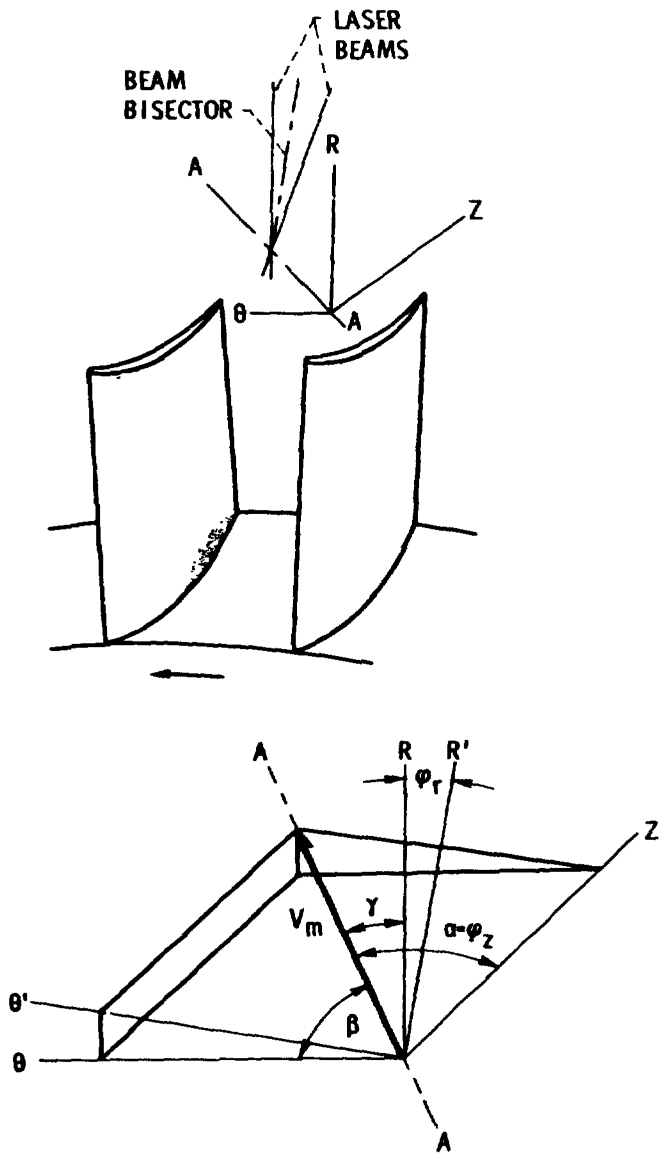

Figure 5. - Coordinate system and LA beam orientation.

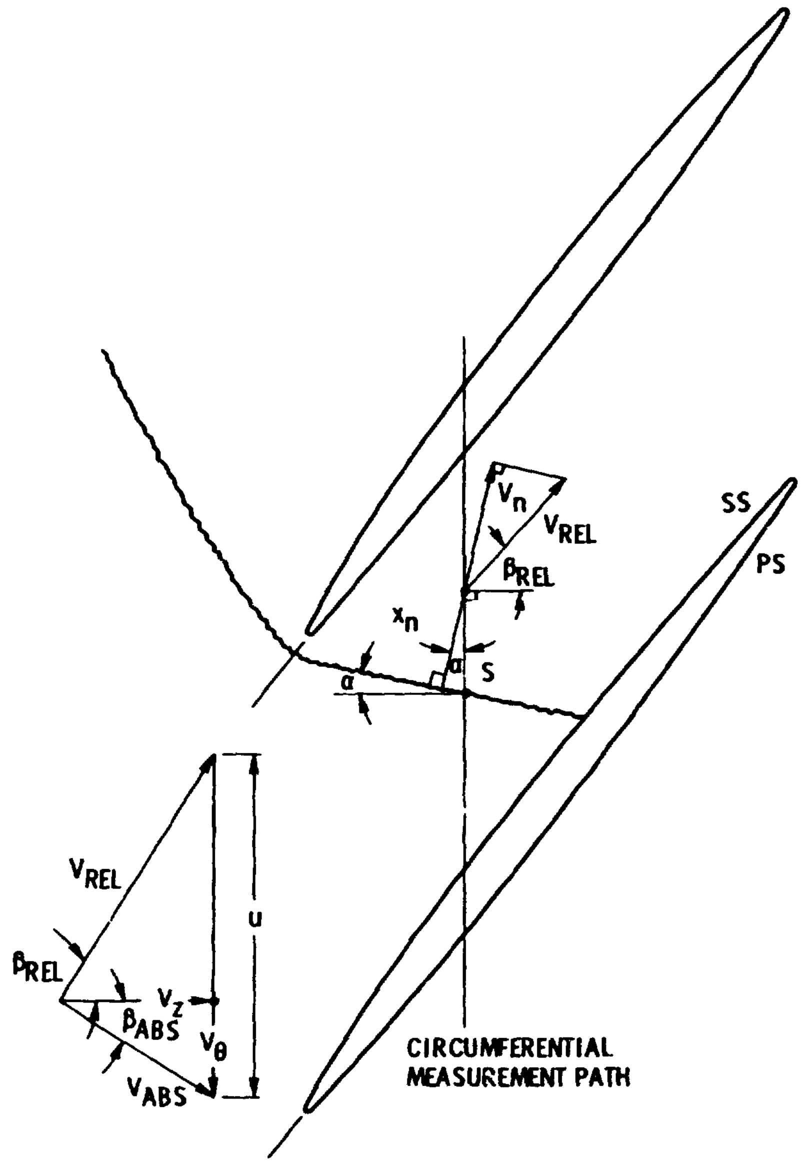

Figure 6. - Relation between the relative velocity V_{REL} and the shock normal velocity component V_n.

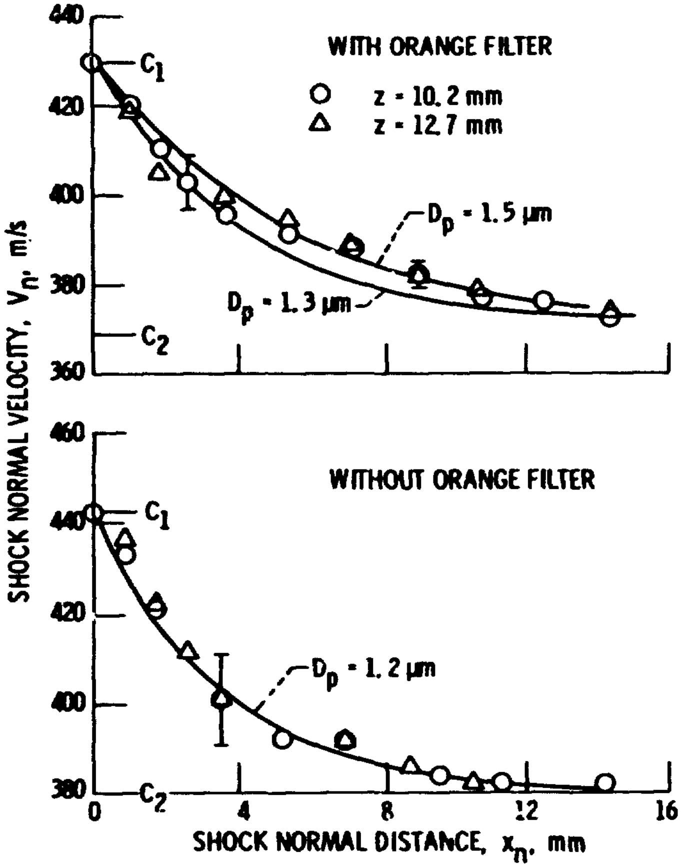

Figure 7. - Seed particle velocity lag downstream of the passage shock. Streamsurface 1, 100% speed, PR = 1.53, W = 205 kg/m^2/s.

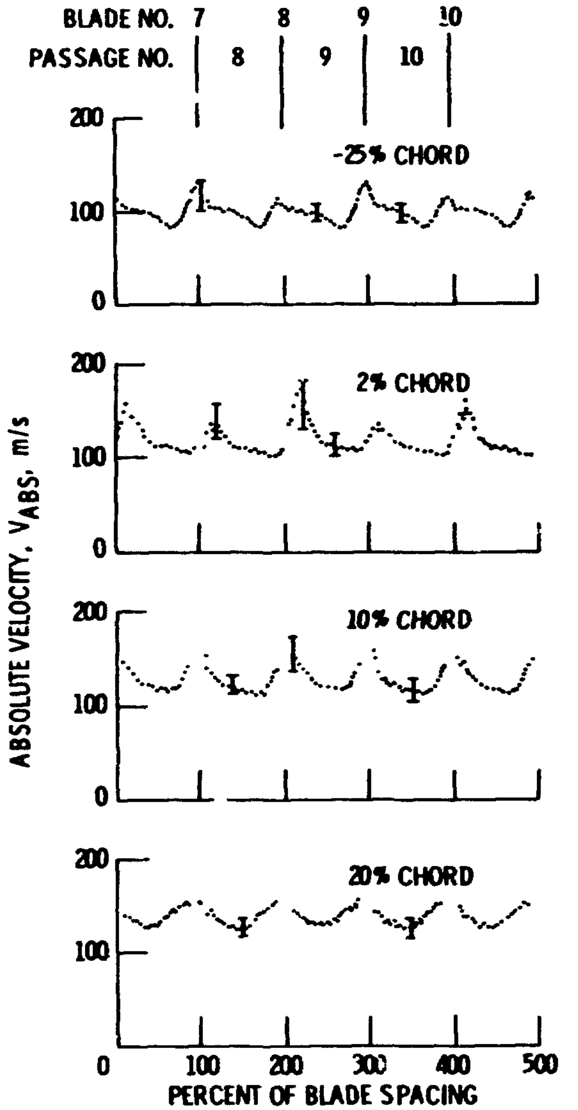

Figure 8. - Passage to passage variation in absolute velocity across five consecutive blade passages. Streamsurface 1, 75% speed, PR = 1.33, W = 123 kg/m^2/s.

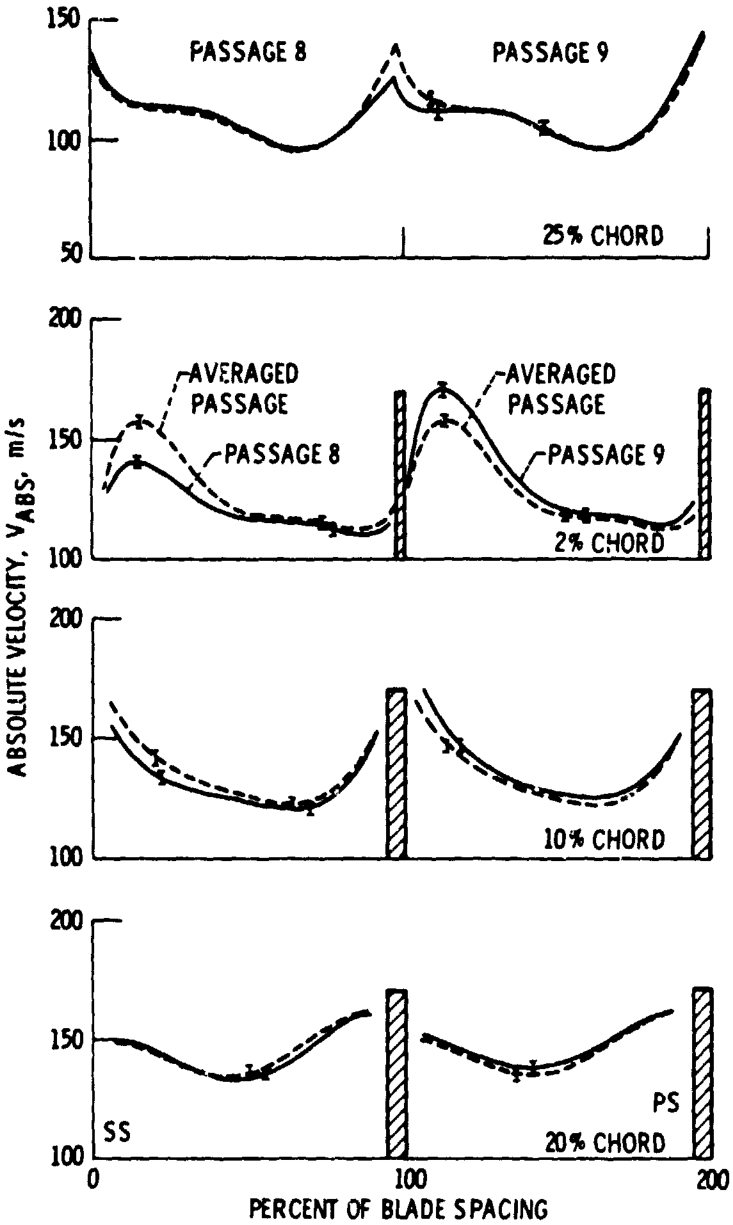

Figure 9. - Comparison between curve fits of the ensemble-averaged and individual blade passage distributions of absolute velocity. Streamsurface 1, 75% speed, PR = 1.33, W = 123 kg/m^2/s.

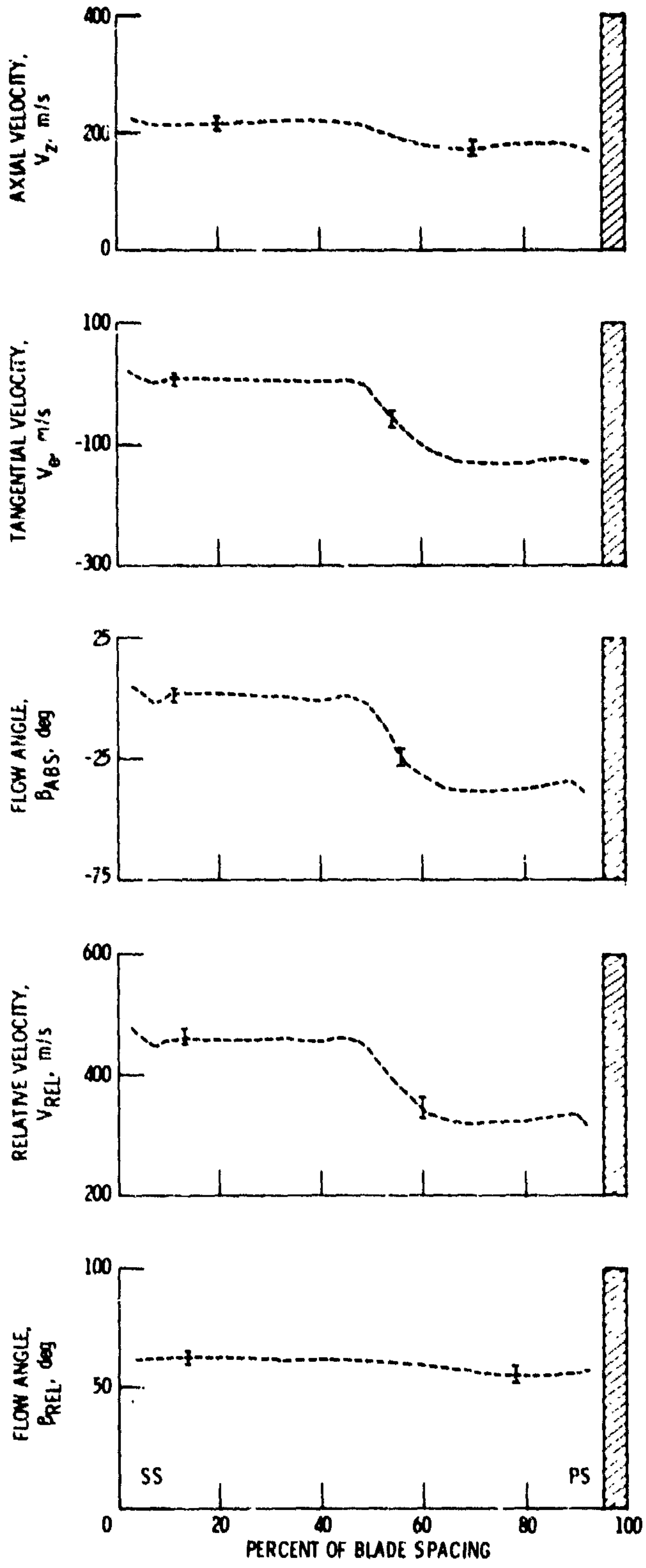

Figure 10. - Ensemble-averaged blade-to-blade distributions of velocity and flow angle across a passage shock. Stream-surface 1, 23% chord, 100% speed, PR = 1.66, W = 190 $kg/m^2/s$.

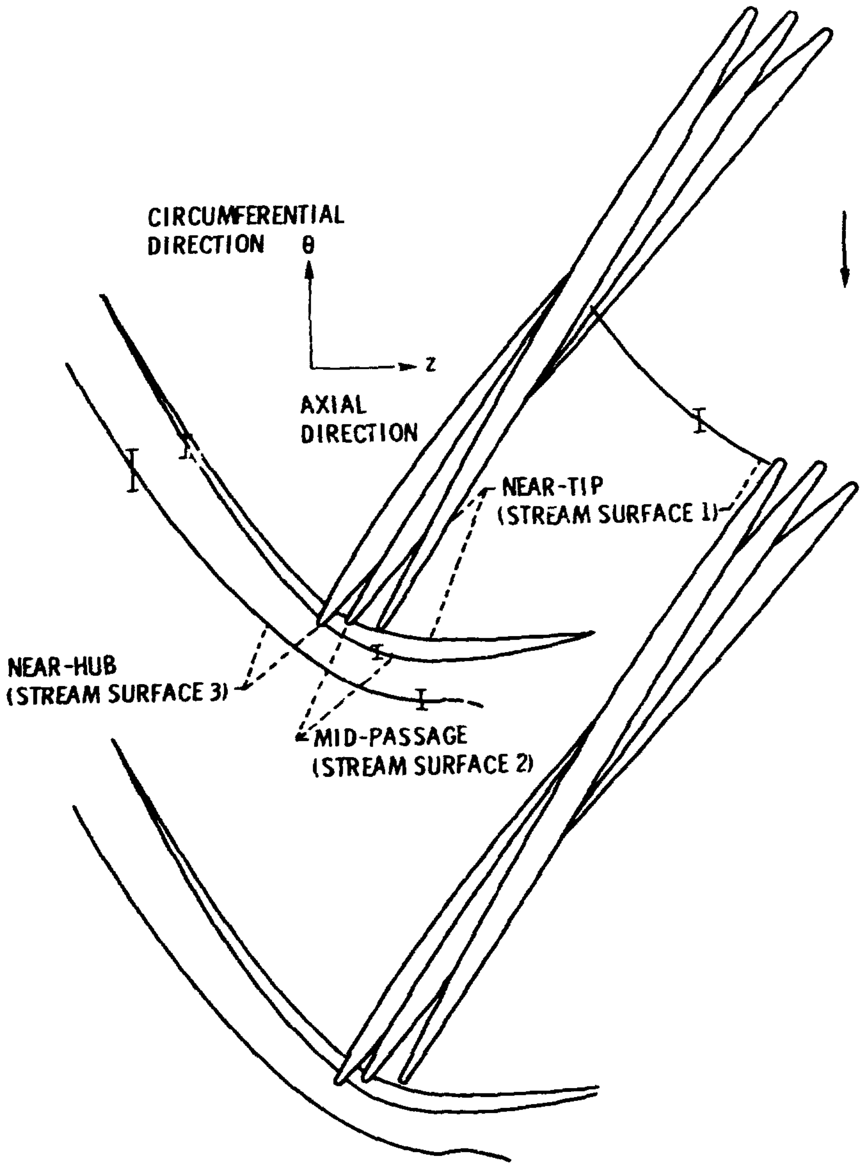

Figure 11. - Three-dimensional structure of the rotor shock system. 100 percent speed, PR = 1.53, W = 205 ks/m^2/s.

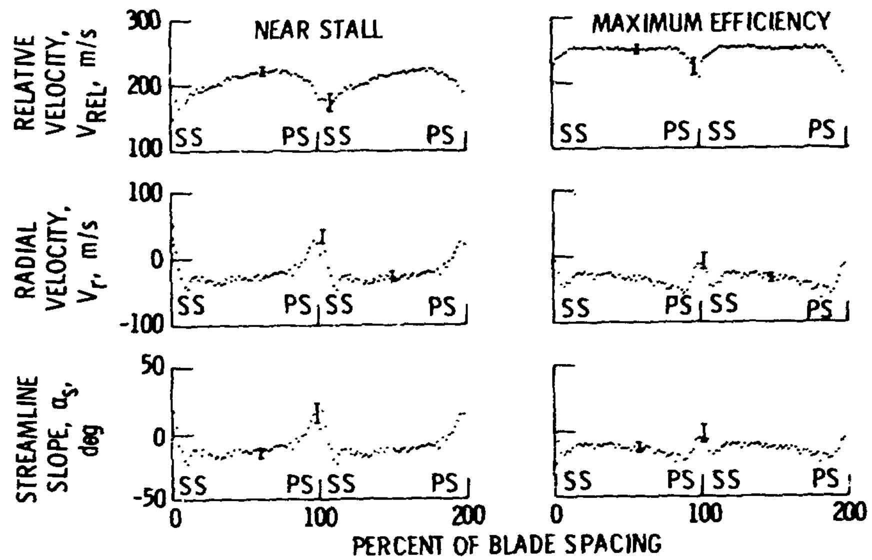

Figure 12. - Ensemble-averaged blade-to-blade distributions of velocity and flow angle in the blade wake. Station 2, stream-surface 1, 70% design speed. Operating conditions: near stall - PR = 1.27, W = 120 kg/m^2/s; maximum efficiency - PR = 1.19, W = 156 kg/m^2/s.

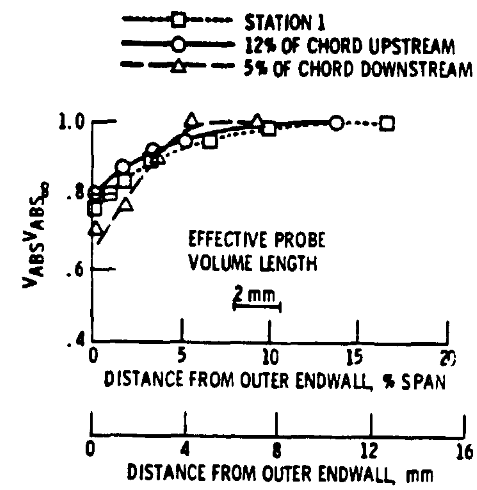

Figure 13. - Development of the outer endwall boundary layer. 100% speed, PR = 1.53, W = 205 kg/m²/s.

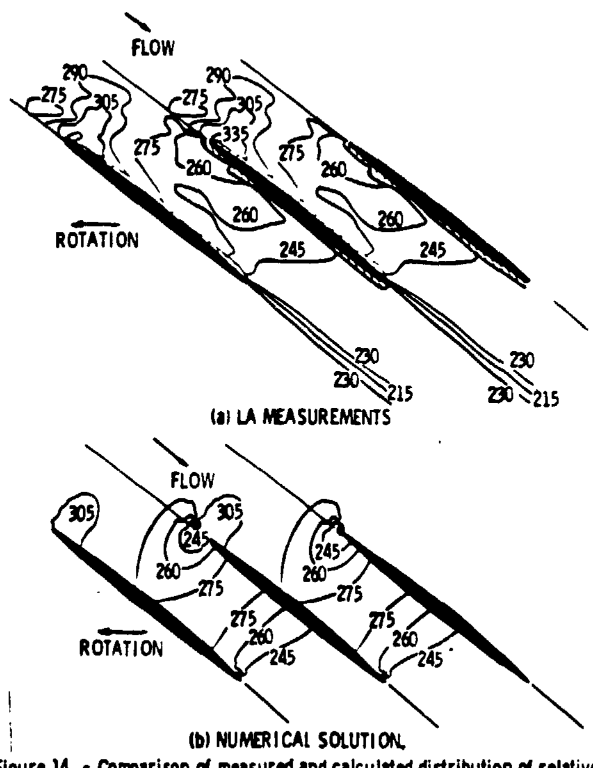

Figure 14. - Comparison of measured and calculated distribution of relative velocity. Stream surface 2, 70 percent speed, PR = 1.19, W = 158 kg/m²/s. Contours in m/s.